RESEARCH ARTICLE

VACCINES

A stable trimeric influenza hemagglutinin stem as a broadly protective immunogen

Antonietta Impagliazzo,[1]*† Fin Milder,[1]‡§ Harmjan Kuipers,[1]‡§ Michelle V. Wagner,[2]‡|| Xueyong Zhu,[3]‡ Ryan M. B. Hoffman,[3]‡ Ruud van Meersbergen,[1]§ Jeroen Huizingh,[1]§ Patrick Wanningen,[1]§ Johan Verspuij,[1]§ Martijn de Man,[1]§ Zhaoqing Ding,[2]|| Adrian Apetri,[1]† Başak Kükrer,[1]† Eveline Sneekes-Vriese,[1] Danuta Tomkiewicz,[1]† Nick S. Laursen,[3]¶ Peter S. Lee,[3] Anna Zakrzewska,[1]§ Liesbeth Dekking,[1]§ Jeroen Tolboom,[1]§ Lisanne Tettero,[1]§ Sander van Meerten,[1]§ Wenli Yu,[3] Wouter Koudstaal,[1]† Jaap Goudsmit,[1]† Andrew B. Ward,[3] Wim Meijberg,[1]§ Ian A. Wilson,[3]* Katarina Radošević[1]#

The identification of human broadly neutralizing antibodies (bnAbs) targeting the hemagglutinin (HA) stem revitalized hopes of developing a universal influenza vaccine. Using a rational design and library approach, we engineered stable HA stem antigens ("mini-HAs") based on an H1 subtype sequence. Our most advanced candidate exhibits structural and bnAb binding properties comparable to those of full-length HA, completely protects mice in lethal heterologous and heterosubtypic challenge models, and reduces fever after sublethal challenge in cynomolgus monkeys. Antibodies elicited by this mini-HA in mice and nonhuman primates bound a wide range of HAs, competed with human bnAbs for HA stem binding, neutralized H5N1 viruses, and mediated antibody-dependent effector activity. These results represent a proof of concept for the design of HA stem mimics that elicit bnAbs against influenza A group 1 viruses.

The ultimate goal of influenza vaccinology is the development of a universal vaccine that protects against a wide range of strains and subtypes, thereby eliminating the need for seasonal reformulation of vaccines and providing an effective defense against viruses with pandemic potential. The relatively recent discovery of broadly neutralizing human monoclonal antibodies (bnAbs) against influenza viruses (*1*–*8*) has raised hopes that a broadly protective vaccine may indeed be feasible (*9*–*13*). Because the majority of these bnAbs are directed toward highly conserved conformational epitopes in the hemagglutinin (HA) stem (*1*, *2*, *4*, *5*, *7*), this region may have the potential to induce broad protective immunity, provided it is well exposed and properly presented.

Various strategies to enhance exposure of the HA stem to the immune system are being explored, including presentation on self-assembling nanoparticles (*14*), chimeric HAs (*15*, *16*), epitope transplantation on a virus-like particle (*17*), and immune refocusing (*18*). Yet another approach involves removal of the HA head while stabilizing the HA stem. A prerequisite for generating a broadly protective soluble HA stem immunogen is that it is stable and structurally resembles the stem of full-length (FL) HA. This simple and elegant concept is complicated by serious structural constraints (*19*). HA is a metastable trimeric surface glycoprotein (*20*, *21*) that undergoes extensive conformational rearrangements at low pH (*22*). Removal of the transmembrane domain and HA head without extensive structural modifications to stabilize the remaining molecule inevitably leads to loss of native conformation of the HA stem (*19*) and concomitant loss of conformational bnAb epitopes. Previously reported soluble HA stem–derived immunogens have exhibited lower affinity with bnAbs relative to FL HA, indicating suboptimal conformation (*23*–*26*).

Design and initial characterization

Starting with the HA sequence of H1N1 A/Brisbane/59/2007, changes were introduced using a combination of rational design and library approaches (*27*). In the first design phase (stages I to III; Fig. 1A), we aimed to generate a soluble and stable HA stem monomer containing bnAb epitopes in the correct conformation, whereas in the final stages (stages IV and V), we aimed to create a mini-HA in its natural trimeric form. Details on the design, sequences, and screening are outlined in (*27*) and figs. S1 and S2. As a readout for a native-like stem conformation of the mini-HA constructs, we used the binding of bnAbs CR9114 and CR6261 (both of which recognize epitopes in the HA stem) (*28*). From each design stage, the best-performing candidates were selected for further optimization. Key mutations in these lead candidates are schematically depicted in fig. S2 and on a model structure of mini-HA in Fig. 1B.

Selected mini-HAs #4157 (stage II), #4454 (stage III), #4650 (stage IV), and #4900 (stage V) were expressed in human embryonic kidney (HEK) 293F cells and purified. On the basis of size, mini-HAs #4157 and #4454 appeared predominantly monomeric in solution; #4650 was larger, suggesting at least partial formation of dimers, whereas #4900 appeared trimeric (fig. S3A). Formation of an intermonomer cysteine bridge in trimeric mini-HA #4900 was confirmed using SDS–polyacrylamide gel electrophoresis under nonreducing and reducing conditions (fig. S3B). All selected mini-HA constructs have four putative N-linked glycosylation sites (Fig. 1B). Under reducing conditions, the mini-HA bands were diffuse and ran at higher molecular weight (35 to 45 kD) than expected (29 kD), indicating that the mini-HAs were glycosylated (fig. S3B). Accordingly, deglycosylation with peptide-N-glycosidase F resulted in sharper bands (~30 kD, as for mini-HA #4900 in fig. S3B). The glycans appear relevant for proper folding, as attempts to efficiently produce mini-HA with retention of bnAb epitopes in bacteria were not successful (*29*).

Size exclusion chromatography with inline multi-angle light scattering (SEC-MALS) analysis revealed a single peak (fig. S4A), with average molecular weights of 40 kD for #4157 and #4454, 60 kD for #4650, and 108 kD for #4900 (Table 1), which also indicated that #4157 and #4454 are monomeric in solution, #4650 forms dimers (at least in part), and #4900 forms trimers. In the presence of CR9114 or CR6261 Fabs, a peak shift to shorter retention time was observed for all mini-HAs, indicating formation of complexes (fig. S4A), which was confirmed by MALS (Table 1), with masses in agreement with binding of one Fab (monomeric mini-HAs #4157 and #4454), one to two Fabs (dimeric mini-HA #4650), or three Fabs (trimeric mini-HA #4900) (*30*).

Binding of CR9114 and CR6261 to all four candidate immunogens was in the nanomolar range, with affinity improving as the design process progressed (Table 1 and fig. S4B). The strongest binding was exhibited by mini-HA #4900, with dissociation constant (K_D) values comparable to those of trimeric FL HA, indicating that this mini-HA recapitulates the bnAb epitopes and thus

[1]Crucell Vaccine Institute, Janssen Center of Excellence for Immunoprophylaxis, Archimedesweg 4-6, 2301 CA Leiden, Netherlands. [2]Crucell Vaccine Institute, Janssen Center of Excellence for Immunoprophylaxis, 3210 Merryfield Row, San Diego, CA 92121, USA. [3]Department of Integrative Structural and Computational Biology, The Scripps Research Institute, 10550 North Torrey Pines Road, La Jolla, CA 92037, USA. ***Corresponding author. E-mail: aimpagli@its.jnj.com (A.I.); wilson@scripps.edu (I.A.W.)** †Present address: Janssen Prevention Center, Janssen Pharmaceutical Companies of Johnson & Johnson, Archimedesweg 4-6, 2301 CA Leiden, Netherlands. ‡These authors contributed equally to this work. §Present address: Infectious Diseases and Vaccines Therapeutic Area, Janssen Research and Development, Janssen Pharmaceutical Companies of Johnson & Johnson, Archimedesweg 4-6, 2301 CA Leiden, Netherlands. ||Present address: Janssen Prevention Center, Janssen Pharmaceutical Companies of Johnson & Johnson, 3210 Merryfield Row, San Diego, CA 92121, USA. ¶Present address: Department of Molecular Biology and Genetics, Aarhus University, Aarhus 8000, Denmark. #Present address: Global Biotherapeutics, Sanofi, 94400 Vitry-sur-Seine, France.

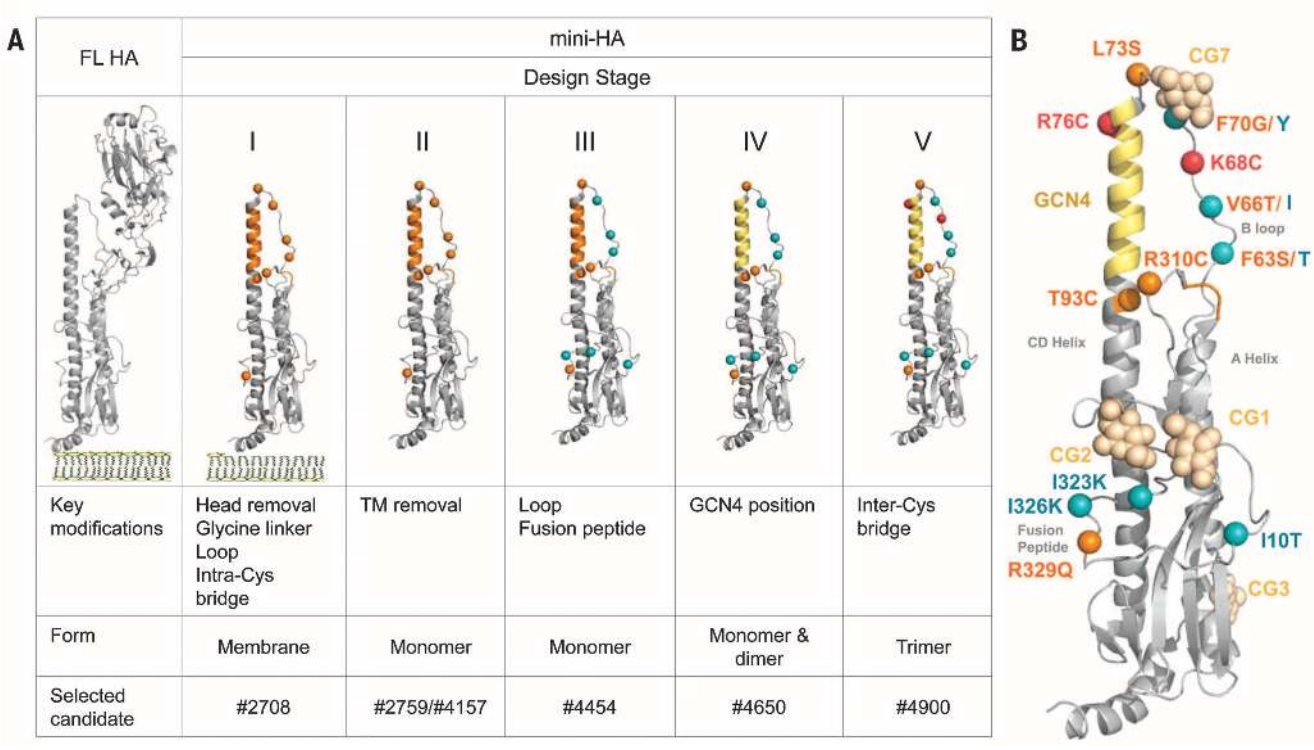

Fig. 1. The mini-HA design strategy and key candidates. (**A**) The mini-HA design strategy is described in five stages, each characterized by specific modifications leading to selection of the best construct for each stage. Key modifications for each stage are schematically depicted and color-coded. Mini-HA #4157 was also generated in an alternative, longer form as mini-HA #2759 with 11 additional C-terminal residues (fig. S1F). (**B**) Ribbon mini-HA model (from PDB ID 1RD8) with color-coded modifications (per stage, as in Fig. 1A) and putative N-glycosylation sites (CG1-3, CG7; taupe).

Table 1. Binding of bnAbs to selected mini-HA candidates. bnAbs CR9114 and CR6261 form high-affinity complexes with mini-HAs. K_D values were determined using biolayer interferometry and steady-state analysis. MALS analysis and size determination were used to confirm Fab binding and complex formation. The numbers are means and SDs of at least two independently produced protein batches. The values in parentheses represent the expected molecular weights for monomeric (#4157, #4454), dimeric (#4650), and trimeric (#4900) mini-HA–Fab complexes, using the determined molecular weight of the mini-HA and 48 kD for the Fabs.

Construct	K_D (nM)		Molecular weight (kD)			
	CR9114	CR6261	Mini-HA	Mini-HA with Fab CR9114	Mini-HA with Fab CR6261	Mini-HA with Fab CR8020
Mini-HA						
#4157	28.3 ± 7.4	490 ± 192	40.3 ± 1.2	78.3 ± 0.6 (88)	63.7 ± 3.2 (88)	42.3 ± 2.1
#4454	9.5 ± 0.7	105 ± 36	40.0 ± 1.4	81.5 ± 2.1 (88)	72.5 ± 2.1 (88)	40.5 ± 2.1
#4650	2.7 ± 0.6	4.5 ± 1.3	59.5 ± 2.1	129.5 ± 2.1 (156)	109.5 ± 0.7 (156)	62.0 ± 1.4
#4900	0.50 ± 0.04	0.6 ± 0.1	107.5 ± 0.7	241.5 ± 0.7 (252)	214.5 ± 2.1 (252)	110.5 ± 0.7
FL HA						
Monomer	6.7 ± 4.0	11.7 ± 4.2				
Trimer	0.8 ± 0.3	0.6 ± 0.2				

accurately mimics the native conformation of the HA stem.

Structural characterization

Modifications introduced throughout the design gradually increased the conformational stability as determined by hydrogen-deuterium exchange mass spectrometry (HDX-MS) (*31*, *32*). In particular, modifications introduced in stage III (from #4157 to #4454) and stage V (from #4650 to #4900) stabilized the overall structure and the shorter A helix (Fig. 2). Furthermore, we observed only a low level of deuterium exchange on the long CD helix of mini-HA #4900, likely due to the shielding effect caused by trimerization. Most important, the HDX pattern of mini-HA #4900 is very similar to that of trimeric FL HA, further demonstrating that the final design mimics the structure and dynamics of native HA. In line with these findings, the overall stability of the mini-HAs also evolved, as is apparent from measurements of the thermal stability (fig. S5).

Complexes of mini-HAs with CR9114 Fab were first studied by negative-stain electron microscopy (EM) (Fig. 3A). The EM class averages illustrate the progression from monomeric (#4454) to a more heterogeneous mixture of monomers and dimers (#4650) and finally to a trimeric form (#4900). To provide further structural insights, we determined the crystal structures of #4454-CR9114 and #4900-CR9114 Fab complexes to 4.3 Å and 3.6 Å resolution, respectively (Fig. 3, B and C, and table S1) (*27*). In the #4454-CR9114 complex (Fig. 3B), CR9114 binds monomeric mini-HA and recognizes essentially the same epitope as in FL HA through contacts only with its heavy chain (table S2) (*11*). The solvent-accessible surfaces of the CR9114 epitope residues in #4900 are similar to those in A/California/04/2009 FL H1 HA (table S3). The #4900 trimer differs only slightly from the stem of trimeric A/California/04/2009 FL HA (and perhaps other HAs), as it adopts a more open, splayed conformation at the trimer base with the HA2 H helix, shifted by about 14.5 Å (Fig. 3, C and D), perhaps as a consequence of insertion of the GCN4 trimerization motif at the top of the long helix in #4900 (fig. S6). The primary amino acid interactions are maintained between CR9114 and #4454 as compared to those between CR9114 and FL H5 HA (*3*), and the CR9114 complex is trimeric

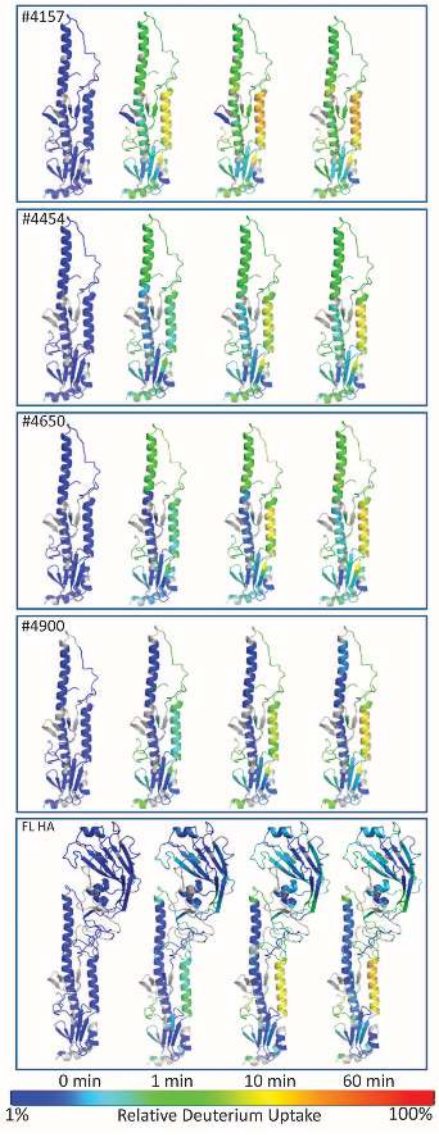

Fig. 2. Dynamic structural properties of mini-HAs and trimeric FL HA analyzed by hydrogen-deuterium exchange mass spectrometry. Relative deuterium uptake over time (0 to 60 min), illustrating the local dynamics of different structural units, is depicted on model mini-HA and FL HA structures using a color code from blue (1% deuterium uptake; highly protected) to red (100% deuterium uptake; highly exposed or flexible).

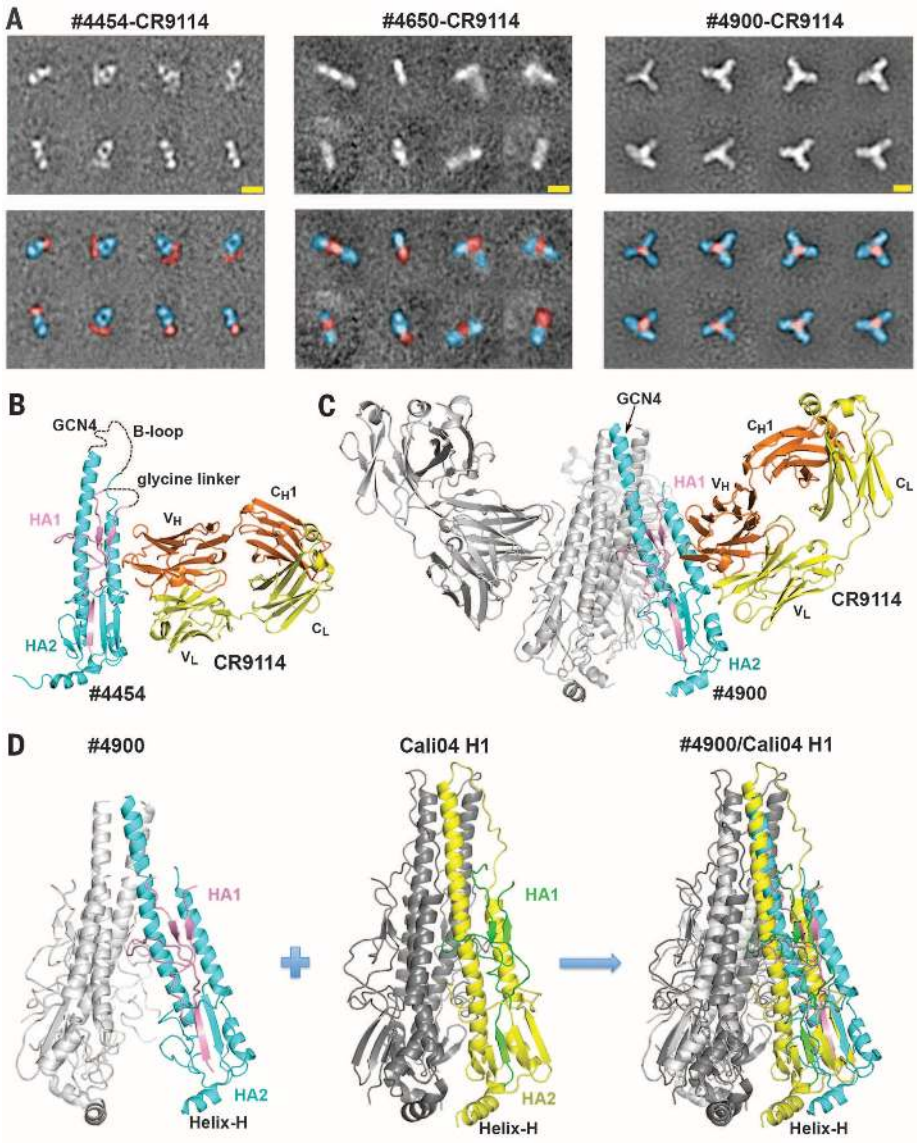

Fig. 3. EM and crystal structures of mini-HAs in complex with CR9114 Fab. (**A**) Representative reference-free class averages of mini-HAs #4454, #4650, and #4900 in complex with CR9114 Fab using negative-stain EM. The colored panels indicate how densities are attributed to either mini-HA (red) or Fab (blue). The yellow scale bar shown is 36.5 Å for the #4454 and #4650 complexes, and 73.0 Å for the #4900 complex. (**B**) Crystal structure of monomeric mini-HA #4454 (pink, HA1; cyan, HA2) in complex with CR9114 Fab (yellow, light chain; orange, heavy chain). The GCN4 motif, the B-loop, and the glycine linker are shown in dashed lines because they are disordered in the structure. (**C**) Crystal structure of trimeric #4900 in complex with CR9114 Fab. One monomer of #4900-CR9114 Fab trimer is shown and color-coded as in (B); the other two monomers of #4900-CR9114 Fab trimer are shown in gray for clarity. The GCN4 motif at the top of the long helix in #4900 is ordered and can be modeled. (**D**) Superimposition of mini-HA #4900 with a "mini-HA" model computationally extracted from the Cali04 HA structure [HA from A/California/04/2009 (H1N1), PDB ID 4M4Y] (one monomer with HA1 in green and HA2 in yellow, and the other two monomers in dark gray). See also tables S2 and S3.

(Fig. 3C). The #4900 protomer is superimposable with an HA protomer from the H1 A/California/04/2009 trimer (PDB ID 4M4Y) with a C_α RMSD of 1.2 Å, and only 1.0 Å for the CR9114 epitope residues. As a consequence of the removal of the HA1 head in #4900 and a more open trimer base (table S2), some residues in the HA2 A helix, B loop, C and D helix, and E strand become solvent-accessible. These results convincingly demonstrate that the iterative design process led to antigens with an increasingly improved HA stem conformation and ultimately yielded HA-like stem antigens with a preserved CR9114 epitope.

In vivo effects

When tested in mice, all mini-HAs were highly immunogenic, eliciting high titers of antibodies binding to the FL HA of the A/Brisbane/59/2007 (H1N1) strain used as the basis for mini-HA generation (fig. S7A), as well as to FL HAs from a number of other group 1 (H1, H5, H9) and group 2 (H3, H7) influenza A strains (fig. S7B). These results demonstrate that antibodies induced with mini-HAs efficiently recognize epitopes that are present in native sequences of FL HA and are

conserved among different group 1 and even some group 2 influenza A strains (*33*).

Next, we evaluated the ability of mini-HA immunogens to provide protection against stringent lethal challenges and characterized the elicited immune response (Fig. 4 and fig. S7). Protection against influenza challenge with H1N1 A/PR/8/34 (heterologous to the parental strain used for design of the mini-HAs) was assessed after one, two, or three immunizations with mini-HAs #2759 (monomer, long variant of #4157; fig. S2), #4650 (mix of monomers and dimers), and #4900 (trimer). Mice immunized three times with monomeric mini-HA #2759 were only partially protected against mortality and showed severe weight loss and clinical symptoms, whereas #4650 and #4900 provided complete protection, with #4900-immunized mice showing neither weight loss nor clinical symptoms (Fig. 4A and fig. S7C). Only mini-HA #4900 showed the same full protective ability when administered twice. Even after one immunization, #4900 exhibited 90% protection against mortality, although animals exhibited some (recoverable) weight loss and clinical symptoms, whereas #4650 and #2759 were not able to protect animals. Antibodies elicited with mini-HA #4900 after two and three immunizations competed with bnAb CR9114 for binding to the FL HA stem (Fig. 4A), which shows that this mini-HA could readily elicit antibodies specific for bnAb stem epitopes.

Mice immunized three times with an expanded set of mini-HAs were challenged with heterosubtypic H5N1 A/Hong Kong/156/97 virus to evaluate the breadth of protection. Mini-HAs #2759 and #4157 (monomers) failed to elicit protection, #4454 (improved library monomer) and #4650 exhibited partial protection, whereas #4900 exhibited complete protection with neither weight loss nor clinical symptoms (Fig. 4B and fig. S7D). To further investigate antibody-mediated effector mechanisms, we tested prechallenge sera in a neutralization assay using pseudoparticles derived from H5N1 A/Vietnam/1194/04 (*34*). Sera from mice immunized with mini-HA #4900, and to some extent #4650, showed detectable neutralization, demonstrating the ability of these mini-HAs to elicit bnAbs (Fig. 4C). Besides direct virus neutralization, Fc-mediated effector mechanisms, such as antibody-dependent cellular cytotoxicity (ADCC), contribute substantially to protection against influenza, with stem-directed bnAbs being particularly effective in these mechanisms (*35*). We therefore used a mouse-adapted ADCC surrogate assay to test prechallenge sera (*36*–*38*). The evolving mini-HAs demonstrated an increasing ability to elicit antibodies with potential to induce ADCC (Fig. 4D), with ADCC potency of serum antibodies corresponding to survival proportions observed in the H5N1 challenge model. In accordance with the binding data (fig. S7, A and B), mini-HA #4900 elicited ADCC responses to a wide range of group 1 influenza A HAs (fig. S7E). To assess whether serum antibodies are indeed responsible for the observed in vivo protection, we passively transferred serum from mice immunized with #4650 and #4900 to naïve mice and subsequently challenged the recipient mice with A/HK/156/97 (H5N1) virus (Fig. 4E and fig. S7F). In contrast to mice that received mock serum, mice that received serum from mini-HA–immunized mice were significantly protected, proving that antibodies play a key role in the protection elicited by mini-HAs.

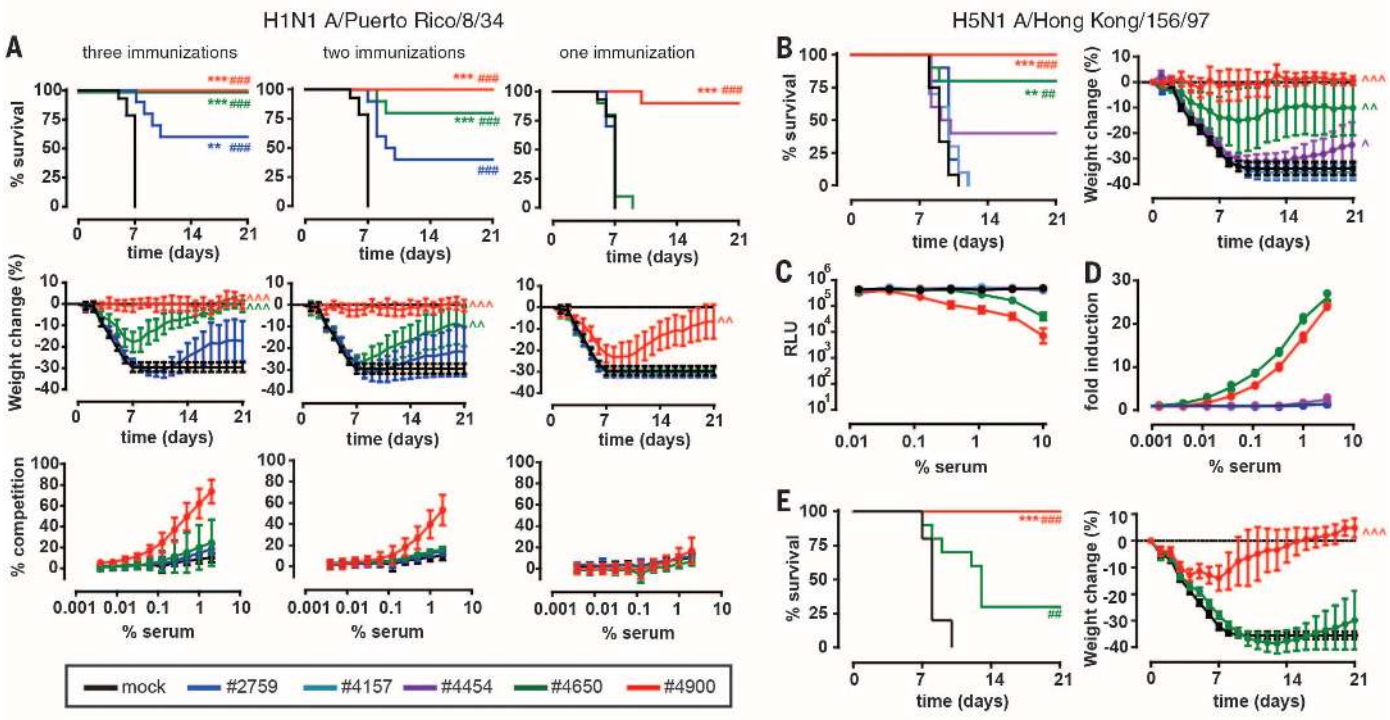

Fig. 4. Immunogenicity and protective efficacy of mini-HA candidates in mice. (**A**) Kaplan-Meier survival curves (top panels) and mean body weight change (middle panels) after one, two, or three immunizations with mini-HA ($n = 10$) or vehicle (mock; $n = 14$), followed 4 weeks later by challenge with 25 times the lethal dose for 50% of mice (LD_{50}) H1N1 A/PR/8/34. Serially diluted prechallenge sera were individually tested for competition with bnAb CR9114 (bottom panels). Error bars denote SD of the mean for CR9114 competition graphs. (**B**) Kaplan-Meier survival curves and mean body weight change of animals ($n = 10$ for mini-HA groups, $n = 12$ for mock group) immunized three times and challenged with 12.5 LD_{50} H5N1 A/Hong Kong/156/97. (**C**) Neutralization of H5 HA A/Vietnam/1194/04 pseudovirus, with prechallenge serum pooled per immunization group. Data shown are geometric means ± SD of three technical replicates per measurement. Results are representative of three independent experiments. (**D**) ADCC surrogate assay with target cells expressing H5N1 A/Hong Kong/156/97 HA and prechallenge serum pooled per immunization group. Individual data points and the line representing the geometric mean of two technical replicates per measurement are shown, representative of two independent experiments. (**E**) Kaplan-Meier survival curves and mean body weight change for animals receiving serum from animals immunized three times with mini-HA or mock ($n = 10$ per group). Four weeks after the last immunization, serum was pooled and transferred to naïve recipient mice on three consecutive days before challenge, followed by challenge with 12.5 LD_{50} H5N1 A/Hong Kong/156/97. Symbols indicate significantly improved survival proportion (Fisher's exact test; *), survival time (log-rank test; #) or body weight change (analysis of variance; ^) relative to mock-immunized animals. Three symbols (i.e., ***, ###, ^^^) indicate $P < 0.001$, two symbols $P < 0.01$, and one symbol $P < 0.05$.

These combined results demonstrate that the progressive structural refinement and stabilization of mini-HAs directly translates to increasing ability to elicit stem-targeting, neutralizing, and ADCC-mediating antibodies that can protect mice against heterologous and heterosubtypic group 1 influenza strains, with trimeric #4900 exhibiting the most favorable features. In a recent study (*26*), a bacterially produced trimeric HA stem construct also seemed more effective than monomeric versions in eliciting protection in an animal influenza challenge model.

We next tested the immunogenicity and protective efficacy of a three-dose regimen of mini-HA #4900 in six cynomolgus monkeys (*Macaca fascicularis*). As controls, groups of six monkeys received three injections of phosphate-buffered saline (PBS) or two human doses of a trivalent seasonal influenza vaccine (the standard of care for naïve children). As previously observed in mice, #4900 elicited high titers of antibodies in monkeys that were able to bind to a wide range of group 1 FL HAs (Fig. 5A and fig. S8A); compete with stem-binding bnAb CR9114 for binding to homologous, heterologous, and heterosubtypic HAs (Fig. 5B); and elicit ADCC responses to these divergent HAs (Fig. 5C). Furthermore, #4900 elicited H5N1 neutralizing antibodies that were detectable not only in a pseudoparticle-based neutralization assay (fig. S8B), as for the mouse sera (Fig. 4C), but also in a standard microneutralization assay (Fig. 5D). Relative to mock-immunized monkeys, animals vaccinated with mini-HA #4900 had significantly reduced fever after challenge with A/Mexico/InDRE4487/2009 (H1N1) virus (Fig. 5E and fig. S8E) (*39*), although no significant effect on the tracheal viral load was detected (fig. S8C). These results are comparable to those from monkeys vaccinated with the trivalent seasonal influenza vaccine (Fig. 5E and fig. S8C). However, the immune response elicited by mini-HA #4900 differed from the response elicited with the trivalent vaccine. As expected, vaccination with the seasonal vaccine, but not with "headless" #4900, elicited hemagglutination-inhibiting (HI) antibodies against A/California/07/09 (H1N1) virus, from which the H1 component of the trivalent vaccine is derived and which is closely related (two amino acid differences) to the A/Mexico/InDRE4487/2009 (H1N1) virus used to challenge the monkeys (fig. S8D). Furthermore, because the A/Texas/50/2012 HA antigen was present in the trivalent seasonal vaccine, the vaccine elicited higher antibody titers against this H3 strain than did mini-HA #4900 (fig. S8A). However, unlike the mini-HA–immunized monkeys, no antibodies able to compete with CR9114, induce ADCC, or neutralize H5N1 virus were detectable in the sera of monkeys immunized with the seasonal vaccine (Fig. 5, B to E, and fig. S8B); these results show that the mini-HA elicited a qualitatively different and much broader immune response than the seasonal vaccine.

In these in vivo studies, we used a single antigen dose and a potent adjuvant. Although this adjuvant has not yet been registered for human use, it has been tested in a number of clinical

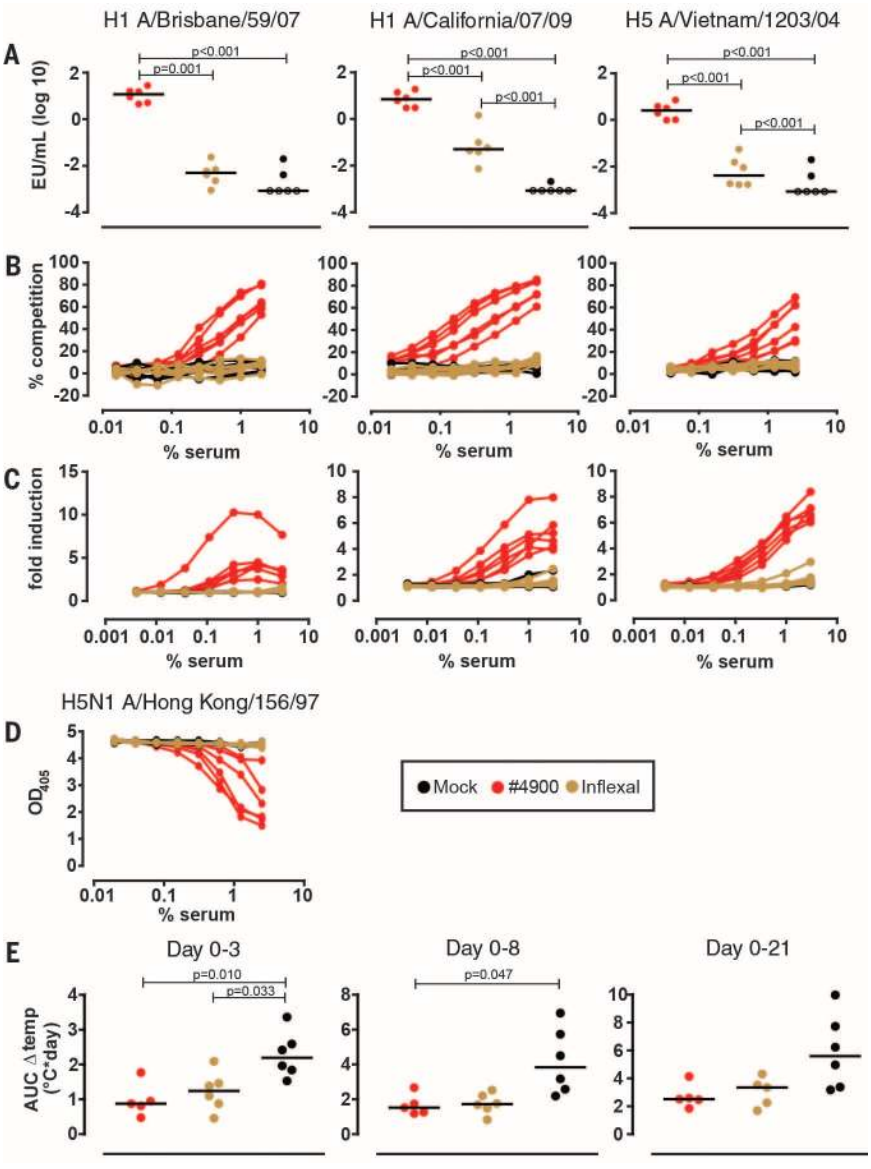

Fig. 5. Immunogenicity and protective efficacy of mini-HA #4900 in cynomolgus monkeys. Animals (n = 6 per group) were immunized with mini-HA #4900, Inflexal V [a trivalent virosomal seasonal influenza subunit vaccine of the 2013 season (H1N1 A/California/07/2009, H3N2 A/Texas/50/2012, and B/Massachusetts/2/2012; 15 μg of HA per strain per vaccine dose], or vehicle (mock) followed by challenge with 4×10^6 median tissue culture infectious dose of H1N1 A/Mexico/InDRE4487/09. (**A**) Prechallenge serum antibody titers to HA from H1N1 A/Brisbane/59/07 (left), H1N1 A/California/07/09 (center), and H5N1 A/Vietnam/1203/04 (right). Open symbols indicate samples that were below detection limits using a serum start dilution of 1/50. Statistical analysis between treatments was performed using pairwise t test with Tukey-Kramer adjustment for multiple comparisons. Bars represent group medians. (**B**) Serially diluted prechallenge sera from individual animals tested for competition with bnAb CR9114, using FL HA from H1N1 A/Brisbane/59/07 (left), H1N1 A/California/07/09 (center), and H5N1 A/Vietnam/1203/04 (right) as antigen. Data shown are the mean of two technical replicates per measurement. (**C**) ADCC surrogate assay with target cells expressing HA from H1N1 A/Brisbane/59/07 (left), H1N1 A/California/07/09 (center), and H5N1 A/Vietnam/1203/04 (right) and prechallenge serum from individual animals. Data shown are the geometric mean of two technical replicates per measurement. (**D**) Neutralization of H5N1 A/Hong Kong/156/97 reassortant virus using serially diluted prechallenge serum from individual animals. Data shown are the mean of two technical replicates per measurement. (**E**) Cumulative net body temperature increase after challenge per animal. The area under the curve of the net temperature increase was calculated over intervals of day 0 to 3 (left), day 0 to 8 (center), and day 0 to 21 (right). Statistical analysis between treatments was performed using pairwise t test with Tukey-Kramer adjustment for multiple comparisons. Bars denote median. One animal of the #4900 group was excluded because of data logger failure, and one animal of the Inflexal group died at the end of day 8 and was excluded from the day 0 to 21 interval calculation.

trials with favorable safety and immunogenicity outcomes (*40*). Future studies will need to address the minimal doses of mini-HA and adjuvant for a protective response. Because preexisting immunity may have a profound effect on the breadth of the response and no animal model recapitulates the complex preexisting immunity against influenza found in humans, such studies should be performed in humans (*41*).

Concluding remarks

We have described the design and characterization of a series of soluble HA immunogens solely composed of the HA stem. Although all selected mini-HAs elicited comparable levels of antibodies to FL HA, the breadth and protective ability of the elicited antibodies progressively increased with the structural evolution of mini-HA configuration. The final candidate—stabilized trimeric mini-HA #4900—demonstrated its unique ability to elicit broad and protective immune response in mice and nonhuman primates. It has been reported (*42*, *43*) that stabilization of respiratory syncytial virus F antigen improves immune response and protection. Our results demonstrate that the same principle holds for influenza HA and provide further direction for the design of an epitope-based, universal influenza vaccine.

REFERENCES AND NOTES

1. D. Corti *et al.*, *Science* **333**, 850–856 (2011).
2. M. Throsby *et al.*, *PLOS ONE* **3**, e3942 (2008).
3. C. Dreyfus *et al.*, *Science* **337**, 1343–1348 (2012).
4. D. C. Ekiert *et al.*, *Science* **324**, 246–251 (2009).
5. D. C. Ekiert *et al.*, *Science* **333**, 843–850 (2011).
6. R. H. Friesen *et al.*, *Proc. Natl. Acad. Sci. U.S.A.* **111**, 445–450 (2014).
7. J. Sui *et al.*, *Nat. Struct. Mol. Biol.* **16**, 265–273 (2009).
8. A. Kashyap *et al.*, *Proc. Natl. Acad. Sci. U.S.A.* **105**, 5986–5991 (2008).
9. D. R. Burton, P. Poignard, R. L. Stanfield, I. A. Wilson, *Science* **337**, 183–186 (2012).
10. G. L. Chen, K. Subbarao, *Nat. Med.* **15**, 1251–1252 (2009).
11. D. C. Ekiert, I. A. Wilson, *Curr. Opin. Virol.* **2**, 134–141 (2012).
12. T. T. Wang, P. Palese, *Nat. Struct. Mol. Biol.* **16**, 233–234 (2009).
13. T. T. Wang, P. Palese, *Science* **333**, 834–835 (2011).
14. M. Kanekiyo *et al.*, *Nature* **499**, 102–106 (2013).
15. R. Hai *et al.*, *J. Virol.* **86**, 5774–5781 (2012).
16. N. Pica *et al.*, *Proc. Natl. Acad. Sci. U.S.A.* **109**, 2573–2578 (2012).
17. A. Schneemann *et al.*, *J. Virol.* **86**, 11686–11697 (2012).
18. D. Eggink, P. H. Goff, P. Palese, *J. Virol.* **88**, 699–704 (2014).
19. J. Cohen, *Science* **341**, 1171 (2013).
20. J. J. Skehel, M. D. Waterfield, *Proc. Natl. Acad. Sci. U.S.A.* **72**, 93–97 (1975).
21. I. A. Wilson, J. J. Skehel, D. C. Wiley, *Nature* **289**, 366–373 (1981).
22. J. J. Skehel *et al.*, *Proc. Natl. Acad. Sci. U.S.A.* **79**, 968–972 (1982).
23. G. Bommakanti *et al.*, *Proc. Natl. Acad. Sci. U.S.A.* **107**, 13701–13706 (2010).
24. G. Bommakanti *et al.*, *J. Virol.* **86**, 13434–13444 (2012).
25. Y. Lu, J. P. Welsh, J. R. Swartz, *Proc. Natl. Acad. Sci. U.S.A.* **111**, 125–130 (2014).
26. V. V. Mallajosyula *et al.*, *Proc. Natl. Acad. Sci. U.S.A.* **111**, E2514–E2523 (2014).
27. See supplementary materials on *Science* Online.
28. CR9114 and CR6261 share a nearly identical epitope formed by helix A of HA2 and a segment of HA1, and both neutralize virtually all group 1 influenza A strains. CR9114 also neutralizes influenza A group 2 viruses and binds influenza B strains, demonstrating greater breadth relative to CR6261. Because CR6261 appears to have more stringent epitope requirements than CR9114, we used CR6261 binding as the key criterion for the selection of final candidates.
29. The apparent importance of the glycans may partially explain why previously reported HA stem–derived proteins that were expressed in *E. coli*, and thus not glycosylated, failed to mimic the native HA stem more closely.
30. SEC-MALS analysis of mini-HAs in combination with Fab of bnAb CR8020, specific for influenza group 2 viruses, showed neither peak shift nor change in retention time for any of the proteins.
31. L. Konermann, J. Pan, Y. H. Liu, *Chem. Soc. Rev.* **40**, 1224–1234 (2011).
32. H. Wei *et al.*, *Drug Discov. Today* **19**, 95–102 (2014).
33. Structural differences between the stems of group 1 and group 2 HAs restrict the activity of most bnAbs to one group. Although some antibodies, like CR9114, can bind both groups, such antibodies appear to be extremely rare. The observed lower reactivity to group 2 HAs of immune serum elicited against group 1 HA stem mimics was therefore to be expected.
34. I. Alberini *et al.*, *Vaccine* **27**, 5998–6003 (2009).
35. D. J. DiLillo, G. S. Tan, P. Palese, J. V. Ravetch, *Nat. Med.* **20**, 143–151 (2014).
36. Z. J. Cheng *et al.*, *J. Immunol. Methods* **414**, 69–81 (2014).
37. B. S. Parekh *et al.*, *MAbs* **4**, 310–318 (2012).
38. A. Schnueriger *et al.*, *Mol. Immunol.* **48**, 1512–1517 (2011).
39. The reduction in fever in #4900-vaccinated animals relative to PBS-immunized animals is significant when periods shortly after challenge (e.g., 0 to 3 days or 0 to 8 days) are considered, because the fever is most pronounced shortly after challenge. Although still visible when the entire 21-day follow-up period is considered, the reduction is no longer statistically significant because of the large variation in measured body temperatures.
40. R. J. Cox *et al.*, *Vaccine* **29**, 8049–8059 (2011).
41. R. Roozendaal *et al.*, *PLOS ONE* **9**, e103550 (2014).
42. B. E. Correia *et al.*, *Nature* **507**, 201–206 (2014).
43. J. S. McLellan *et al.*, *Science* **342**, 592–598 (2013).

ACKNOWLEDGMENTS

We thank R. Vogels, R. van der Vlugt, D. Zuijdgeest, N. Kroos, V. Klaren, S. Schmit-Tillemans, L. Kil, S. Barens, and O. Diefenbach for scientific input and technical support; J. Klap, M. Koldijk, and G. J. Weverling for statistical support; Algonomics for input in early designs; Novavax for supplying Matrix-M; Promega for early access to mouse surrogate ADCC assay; E. Montomoli, D. Perini, and S. Piccirella from VisMederi for pseudoparticle assay; Janssen Diagnostics for quantitative polymerase chain reaction of tracheal swabs; P. Mooij and G. Koopman of the Biomedical Primate Research Center (BPRC), TNO Triskelion, Central Veterinary Institute, and PreClinBiosystems AG for performing the animal studies; and L. Dolfing and A. Dingemans for critical reading of the manuscript. The data presented in this manuscript are tabulated in the main paper and in the supplementary materials. X-ray diffraction data sets were collected at the Stanford Synchrotron Radiation Lightsource (SSRL) beamline 12-2. Use of the SSRL, SLAC National Accelerator Laboratory, is supported by the U.S. Department of Energy (DOE), Office of Science, Office of Basic Energy Sciences under contract no. DE-AC02-76SF00515. The SSRL Structural Molecular Biology Program is supported by the DOE Office of Biological and Environmental Research and by National Institute of General Medical Sciences (NIGMS) grants including P41GM103393. The contents of this publication are solely the responsibility of the authors and do not necessarily represent the official views of NIGMS or NIH. Coordinates and structure factors of the crystal structures are deposited in the Protein Data Bank as entries 5CJQ and 5CJS. Crucell Holland B.V., a Janssen company, has the following pending patent applications in this field: WO 2013/079473, WO 2014/191435, WO2008/028946, WO2013/007770, U.S. 62/062,746, and U.S. 62/062,754. Sharing of materials will be subject to standard material transfer agreements.

SUPPLEMENTARY MATERIALS

www.sciencemag.org/content/349/6254/1301/suppl/DC1
Materials and Methods
Figs. S1 to S8
Tables S1 to S3
References (*44*–*65*)

26 November 2014; accepted 29 July 2015
Published online 24 August 2015
10.1126/science.aac7263

REPORTS

METALLIC GLASSES

Fractal atomic-level percolation in metallic glasses

David Z. Chen,[1]* Crystal Y. Shi,[2]† Qi An,[3]† Qiaoshi Zeng,[4,5] Wendy L. Mao,[2,6] William A. Goddard III,[3] Julia R. Greer[1,7]

Metallic glasses are metallic alloys that exhibit exotic material properties. They may have fractal structures at the atomic level, but a physical mechanism for their organization without ordering has not been identified. We demonstrated a crossover between fractal short-range (<2 atomic diameters) and homogeneous long-range structures using in situ x-ray diffraction, tomography, and molecular dynamics simulations. A specific class of fractal, the percolation cluster, explains the structural details for several metallic-glass compositions. We postulate that atoms percolate in the liquid phase and that the percolating cluster becomes rigid at the glass transition temperature.

Freeze a liquid fast enough, and it becomes a glass, a material that is structurally similar to the liquid but incapable of flow. This concept, albeit not well understood (*1*, *2*), is so ubiquitous that it holds even for metals (*3*). Vitrified metals, or metallic glasses, are a class of disordered materials with nondirectional bonding and possess a suite of lucrative mechanical properties, such as high elastic limit and strength (*4*). Unlike most crystalline metals and alloys, metallic glasses earn their name from a lack of long-range atomic order and the absence of typical defects, such as dislocations, rendering their microstructure challenging to conceptualize